J Appl Electrochem (2008) 38:853–859
DOI 10.1007/s10800-008-9523-5

ORIGINAL PAPER

Galvanic corrosion of titanium-based dental implant materials

Halit Arslan · Hüseyin Çelikkan · Nisa Örnek · Oğuz Ozan · A. Ersan Ersoy · M. Levent Aksu

Received: 16 July 2007 / Revised: 8 February 2008 / Accepted: 18 February 2008 / Published online: 28 February 2008

Abstract This paper describes an investigation of the corrosion behavior of Ti-based dental materials with Au, CrNi and CoCr in Ringer solution by the use of Tafel plots, Evans diagrams and EIS Nyguist diagrams. The galvanic potentials and currents obtained for various implant couples are as follows: For, Ti6Al4V/CrNi couple −0.030 V (Ag/AgCl (3 M NaCl)) and 7.94 μA cm^{-2}; for Ti6Al4V/CoCr couple −0.020 V (Ag/AgCl (3 M NaCl)) and 7.08 μA cm^{-2}; for Ti6Al4V/Au couple −0.020 V (Ag/AgCl (3 M NaCl)) and 5.62 μA cm^{-2}. The Ti6Al4V/Au couple was found to be the most suitable one against galvanic corrosion according to both the Tafel method and mixed potential theory. The corrosion behaviors of Ti6Al4V/CoCr and Ti6Al4V/CrNi couples were found to be similar.

Keywords Galvanic corrosion · Ti-based dental materials · Tafel plots · Electrochemical impedance spectroscopy

H. Arslan
Department of Chemistry, Art and Science Faculty, Gazi University, 06500 Besevler, Ankara, Turkey

H. Çelikkan
Mineral Research and Exploration Institute, Balgat, Ankara, Turkey

N. Örnek · O. Ozan · A. E. Ersoy
Faculty of Dentistry, Ankara University, 06500 Besevler, Ankara, Turkey

M. L. Aksu (✉)
Department of Chemical Education, Gazi Education Faculty, Gazi University, 06500 Besevler, Ankara, Turkey
e-mail: maksu@gazi.edu.tr

1 Introduction

Titanium and its alloys have been widely used in restorative surgery such as dental and orthopedic prostheses, pacemakers and heart valves [1] due to their excellent mechanical properties, good corrosion resistance and biocompatibility in biological fluids [2]. The contact between the metallic implant and the receiving living tissues is made through the oxide layer on the implant surface, which allows the osseointegration process [3]. Titanium is a relatively new material used for surgical purposes [4, 5]. Titanium undergoes an allotropic transformation from a hcp structure (α-phase) to a bcc structure (βphase) at 882 °C [6].

The corrosion of the in vivo implant materials may be the source of harmful material in the body and deterioration of the biomaterials [7]. CoCr, CrNi, and Ti are the most widely used materials in dental implants. Among these are Ti alloys which are particularly popular due to their chemical inertia [8], mechanical strength [9], low toxicity and lightness [10], and excellent biocompatibility [7].

The Ti-based implant materials owe their high corrosion resistance to the passive layer formed on their surfaces which contain mainly amorphous titanium dioxide [11–13]. The physico-chemical and electrochemical properties of this film and its long-term stability in biological environments play a decisive role for the biocompatibility of titanium implants [14].

This layer dissociates according to the following mechanism [15]:

$$TiO_2 + H_2O + H^+ \rightarrow Ti(OH)_3^+$$

The dissolved oxygen present in body tissues also promotes corrosion of the implant material as a result of two different cathodic reactions according to the pH of the medium:

$$O_2 + 2H_2O + 4e \rightarrow 4OH^-$$

$$O_2 + 4H^+ + 4e \rightarrow 2H_2O$$

The complexity of the electrochemical processes involved in the implant-suprastructure joint is linked to the phenomena of galvanic coupling and pitting corrosion [16]. The Cl^- and F^- anions present in the medium increase the corrosion rate to a significant extent by the dissolution of the passive layer. This is especially important for dental materials due to fluoride in toothpastes [17].

It was established by Tomashov [18] that anodic dissolution in the active–passive transition state of the biphase Ti–Mo alloys (and it is reasonable to presume that this phenomenon takes place for all the alloys) takes place by a selective dissolution of the α-phase and simultaneous reprecipitation of the β-phase.

It has been reported [7] that the surface film in the human body changes in thickness and composition with time. So, simulation of long-term exposure of implants using various electrochemical techniques could be a help for prediction of in vivo behavior. Despite the high corrosion resistance of titanium and its alloys, in vivo experiments showed accumulation of titanium ions in tissue adjacent to implants [19, 20].

One important fact which must be taken into account in the use of implant materials is galvanic corrosion as a result of contact with two different materials. There are various techniques employed for the investigation of corrosion of implant materials such as Tafel method [21] and electrochemical impedance spectroscopy (EIS) [22, 23]. The high resistance implies a high corrosion resistance C_p, i.e., a low rate of titanium release and oxide growth.

The decrease in size of the capacitive semicircle indicates increased dissolution. The rate of the overall process depends on the rates of the following processes: (i) formation of oxide at the metal/oxide interface; (ii) transport of either metal or oxygen vacancies across the film; (iii) generation or consumption of vacancies at the oxide/electrolyte interface; (iv) chemical or electrochemical dissolution process [24]. Noble metals catalyze the reduction of oxygen and water causing an increase in the cathodic efficiency. This shifts the potential to the positive direction and the formed oxide film will be thicker [25]. The addition of beneficial alloying elements that facilitate cathodic depolarization by providing sites of low hydrogen overvoltage will cause the potential of the alloy to shift to the noble direction where oxide film passivation is possible [26]. There is substantial evidence that oxide film on Ti metal and its alloys in many exposure conditions exhibit a two-layer structure, one dense inner layer and a porous outer layer [27, 28]. The passive films on Ti were characterized by EIS as follows [29–31]:

Circuits I and II (shown in Fig. 1) have been proposed to represent the unsealed and sealed anodic oxides respectively [32]. For the unsealed anodic oxide film it is generally agreed that the pores in the outer porous layer are filled with electrolyte while for the sealed oxide the pores re filled with the hydrated oxide. In the latter case the hydrates inside pores need to be taken into account in the equivalent circuit and the inner layer may be approximated as a capacitance.

In this study the corrosion of the Ti6Al4V jaw material and porcelain substructure materials such as CoCr, CrNi, Au were investigated in Ringer's solution at 37 °C (Table 1) [33]. The corrosion potentials and currents of the jaw material and porcelain substructure materials were compared to find galvanic potential (E_{couple}) and galvanic current (I_{couple}) values of galvanic couple. For each alloy relevant equivalent circuits have been proposed.

2 Materials and methods

2.1 Corrosion tests

All the corrosion tests were carried out at 37 °C in Ringer's solution (0.31 g Sodium lactate, 0.02 g Calcium chloride, 0.6 g Sodium chloride and 0.03 g Potassium chloride in 100 mL water). The temperature of the solution was controlled by the use of a Nuve thermostat (Ankara/Turkey). The corrosion cell was purged with purified N_2 for ten minutes prior to each experiment in order to remove the residual oxygen. The solution was stirred with a magnetic stirrer.

2.2 Samples

The corrosion behavior of five different types of dental implant material was investigated. The surface areas of the specimens were almost the same and their compositions are given in Table 1.

The working electrodes were prepared by covering the edges with polyester exposing a certain surface area. The surfaces were firstly polished with 500, 700, and 1,200 grit emery paper and 0.5 μm alumina to a mirror finish and washed with de-ionized water before being placed in the corrosion cell.

2.3 Electrochemical measurements

All the electrochemical measurements were made using a computer controlled CH Instruments 660 B Electrochemical

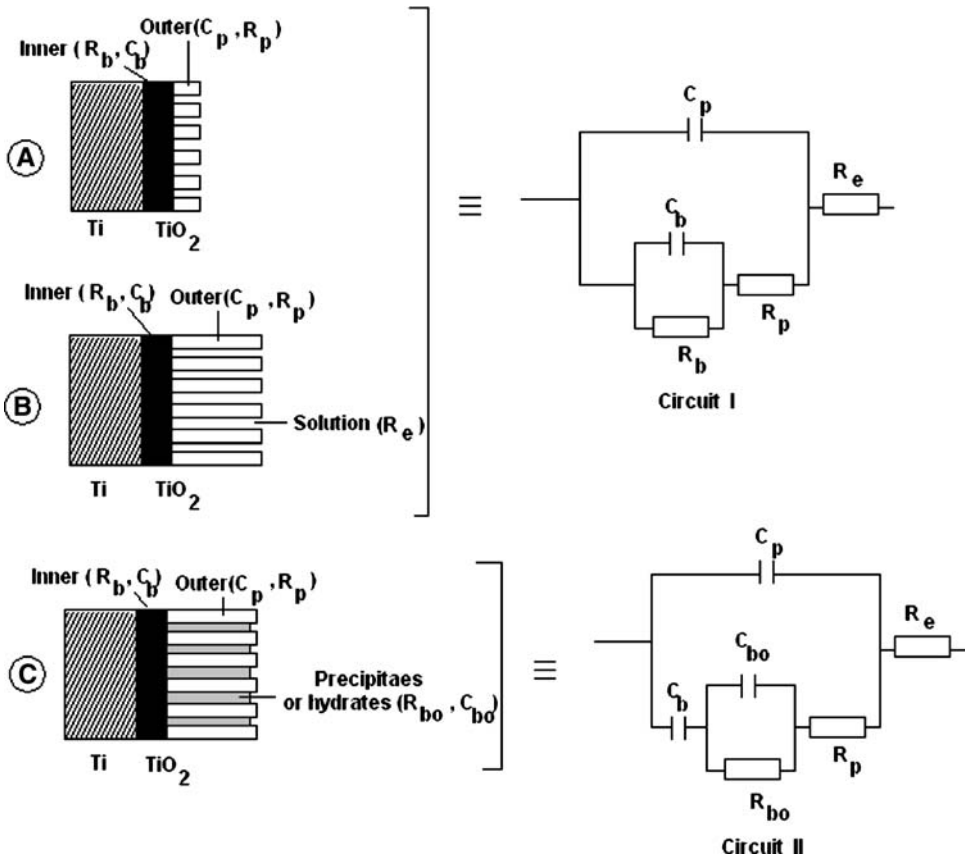

Fig. 1 Equivalent circuits representing unsealed and sealed oxides

Table 1 Composition of working alloys

Types of the alloys	Compositions % (max)
Ti implant	N:0.05, C:0.08, H:0.012, Fe:0.25, O:0.13, Al:5.5–3.5, V.3.5–4.5, Ti: remaining
Au alloy	Fe:0.25, O:0.20, N:0.06, C:0.08, H:0.013, Au: remaining
Co–Cr alloy	Co:64.8, Cr:28.0, Mo:5.0, Si, Mn, C, Ni and N < 1.0 (each)
Cr–Ni alloy	Ni:63.0, Cr:24.7, Mo:10.8, Si:1.5, Mn:0.01, C:0.03

Analyzer using a three electrode cell with a 1 cm^2 Pt plate auxiliary and Ag/AgCl (3 M NaCl) reference electrodes. The anodic and cathodic Tafel slopes were plotted between −300 mV to +300 mV from the equilibrium potential at a scan rate of 2 mV s^{-1} after the initial potential of the system reached equilibrium.

EIS plots were taken with an electrode brought to open circuit equilibrium potential by applying a sinusoidal wave with a frequency ranging from 0.02 to 10,000 Hz and the data were represented as Nyquist diagrams taking the surface areas into account. The data collected were simulated by the use of Zsimpwin software giving the relevant equivalent circuits. The values of the electrical components are tabulated in Table 2.

2.4 Determination of galvanic corrosion using polarization curves

In order to find galvanic corrosion potentials and currents the anodic polarization curves of the dental material obtained by the Tafel method were superimposed onto each other. The difference in the corrosion potentials and the corrosion currents of the superimposed curves are directly proportional to the magnitude of the galvanic corrosion. In order to find the quantitative value of the galvanic corrosion the coincidence point of the anodic polarization curve with the more negative corrosion potential and the cathodic polarization curve with more positive corrosion potential was determined. The current and potential at this point represent the galvanic corrosion current (I_{couple}) and the galvanic corrosion potential (E_{couple}).

2.5 Galvanic corrosion by application of the mixed potential theory

As described in Sect. 2.4 the Tafel slopes of each material were separately determined and the coincidence point of

Table 2 Values of electrical components of the equivalent circuits drawn according to EIS data

	Ti alloy	Au alloy	CoCr alloy	CrNi alloy
R_1/ohm cm^{-2}	20	21	3,8	34
R_2/ohm cm^{-2}	5.60×10^5	3.22	40.0	207.9
R_3/ohm cm^{-2}	1.13×10^6	2,640	5×10^{12}	1.61×10^5
R_4/ohm cm^{-2}	7.70×10^9	–	–	–
C/F cm^{-2}	5.35×10^{-5}	6.60×10^{-5}	–	1.85×10^{-5}
Q_1, Yo/S $s^{1/2}$ cm^{-2}	1.47×10^{-10}	2.38×10^{-4}	5.62×10^{-5}	4.73×10^{-5}
	$n = 0.99$	$n = 0.62$	$n = 0.80$	$n = 0.80$
Q_2, Yo/S $s^{1/2}$ cm^{-2}	5.43×10^{-9}	–	5.0×10^{-9}	–
	$n = 0.66$		$n = 0.90$	
W_1, Yo/S $s^{1/2}$ cm^{-2}	–	–	7.27×10^{-5}	–
W_2, Yo/S $s^{1/2}$ cm^{-2}	–	–	–	–

the anodic section of the material with the more negative corrosion potential with the cathodic section of the material with more positive corrosion potential corresponds to galvanic corrosion current (i_{couple}), and galvanic corrosion potential (E_{couple}).

3 Results and discussion

3.1 Galvanic corrosion of the metal couples by the use of anodic polarization method

As seen from Figs. 2, 3, 4 Ti6Al4V and CrNi alloys are extremely resistant against corrosion and their corrosion potentials are highly positive. Ti6Al4V owes this corrosion resistance to the passive oxide surface layer (TiO_2). However when it is in contact with CrNi alloys the corrosion potential shifts negatively and the materials become much more susceptible to corrosion. The galvanic corrosion potential and current of Ti6Al4V and CrNi alloys are tabulated in Table 3.

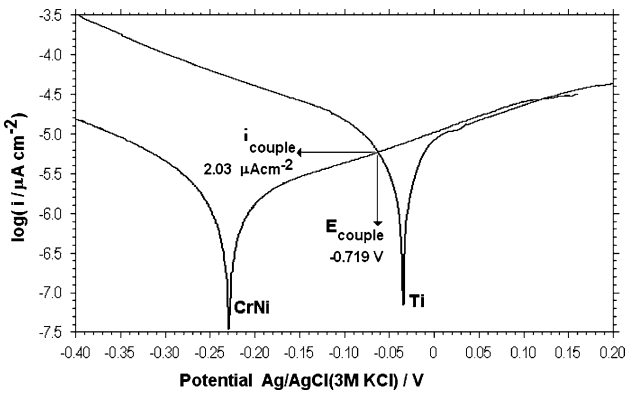

Fig. 2 Galvanic corrosion current (i_{couple}) and galvanic corrosion potential (E_{couple}) for Ti6Al4V and CrNi implant materials by the use of Tafel method

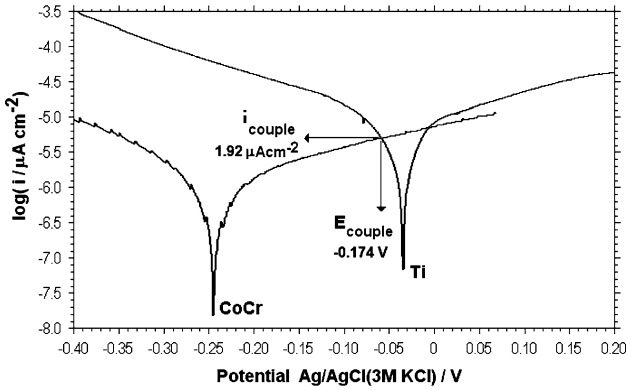

Fig. 3 Galvanic corrosion current (i_{couple}) and galvanic corrosion potential (E_{couple}) for Ti6Al4V and CoCr implant materials by the use of Tafel method

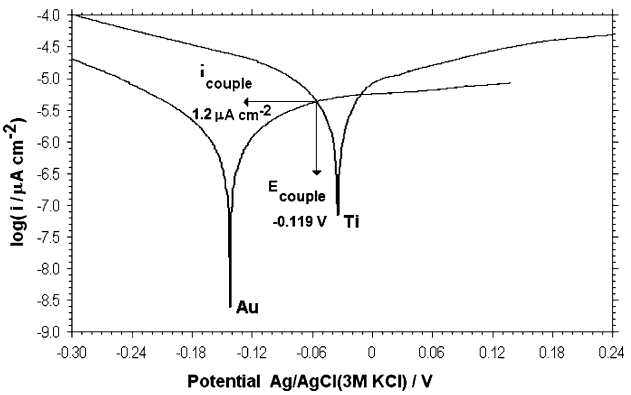

Fig. 4 Galvanic corrosion current (i_{couple}) and galvanic corrosion potential (E_{couple}) for Ti6Al4V and Au implant materials by the use of Tafel method

3.2 The galvanic corrosion results by the application of the mixed potential theory

The galvanic corrosion currents and potentials obtained by the application of mixed potential theory are similar to

Table 3 Galvanic corrosion currents and potentials of various implant materials

Galvanic couples	Corrosion parameters obtained with the Tafel method		Corrosion parameters obtained with the mixed potential theory	
	E_{couple}/V vs Ag/AgCl(3M)	I_{couple}/μA cm^{-2}	E_{couple}/V vs Ag/AgCl(3M)	I_{couple}/μA cm^{-2}
Ti–CoCr	−0.174	1.92	−0.020	7.08
Ti–CrNi	−0.179	2.03	−0.030	7.94
Ti–Au	−0.119	1.20	0.020	5.62

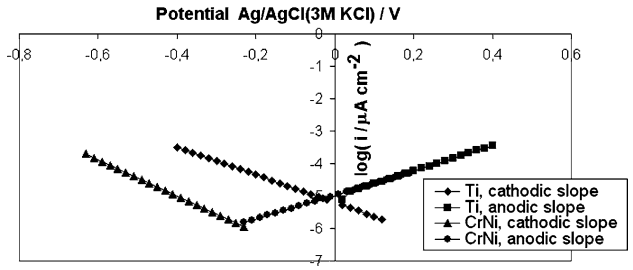

Fig. 5 Galvanic corrosion potential (E_{couple}) and current (i_{couple}) for Ti6Al4V and CrNi implant materials by the use of mixed potential theory

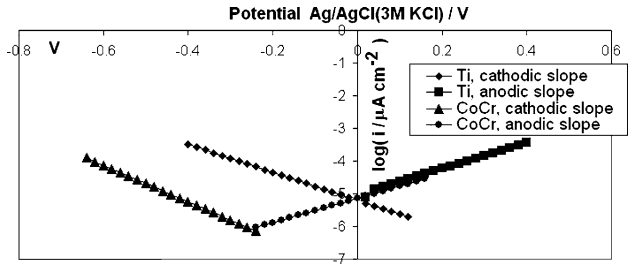

Fig. 6 Galvanic corrosion potential (E_{couple}) and current (i_{couple}) for Ti6Al4V and CoCr implant materials by the use of mixed potential theory

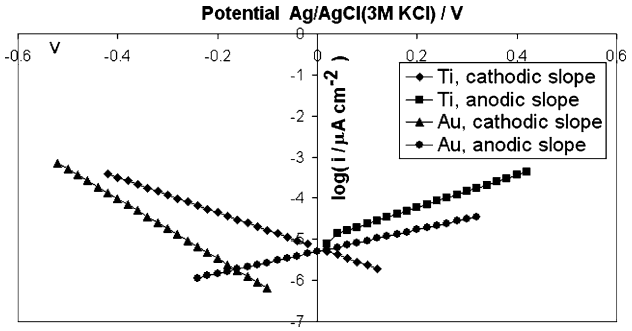

Fig. 7 Galvanic corrosion potential (E_{couple}) and current (i_{couple}) for Ti6Al4V and Au implant materials by the use of mixed potential theory

those found with Tafel plots (Figs. 5, 6, 7). The galvanic potentials and currents are tabulated in Table 3. The Ti6Al4V/Au couple has the highest resistance to galvanic corrosion according to both the Tafel method and mixed potential theory.

3.3 The electrochemical impedance spectroscopy (EIS) data of the materials

The EIS data are depicted as Nyquist diagrams in Figs. 8–11.

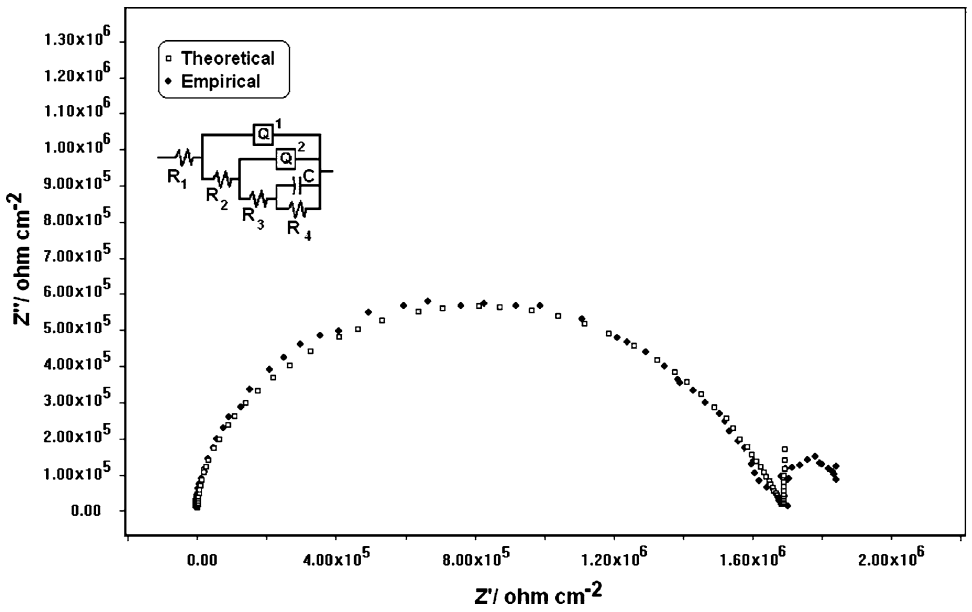

Fig. 8 Experimental and simulated Nyquist diagrams of Ti6Al4V alloy in Ringer solution

The Nyquist diagram of the Ti6Al4V alloy (Fig. 9) gives a full capacitive loop with two time constants. This is indicative of a two layered oxide film with a compact inner layer and a porous outer layer. The complexity of the associated equivalent circuit with two time constants shows that the pores are sealed with the hydrated material. The correlation between the experimental and simulated loops is well over 95%

A non-closing capacitive loop (Fig. 9) is an indication of the oxide layer dissolution. The reaction is diffusion controlled as indicated by the addition of a Warburg impedance to the charge transfer resistance corresponding to mass transfer and diffusion limitations. This is due to the fact that the oxide is not strongly bound to the surface and shows rapid dissolution.

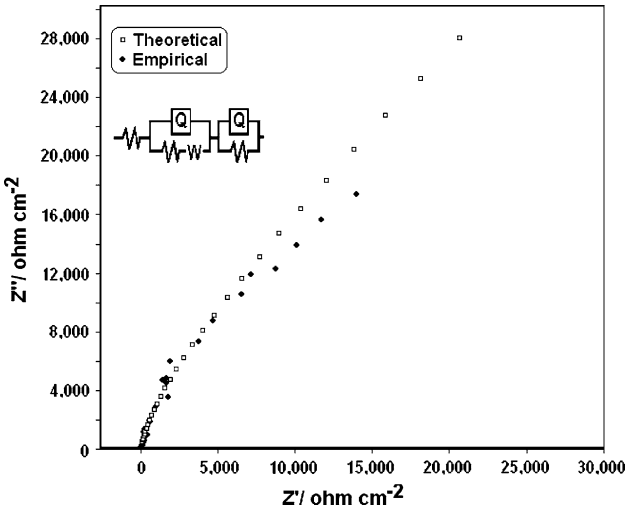

Fig. 9 Experimental and simulated Nyquist diagrams of CoCr in Ringer solution

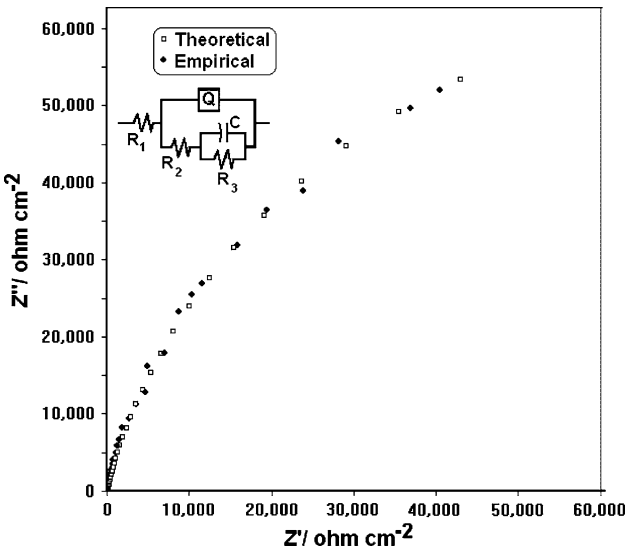

Fig. 10 Experimental and simulated Nyquist diagrams of CrNi alloy in Ringer solution

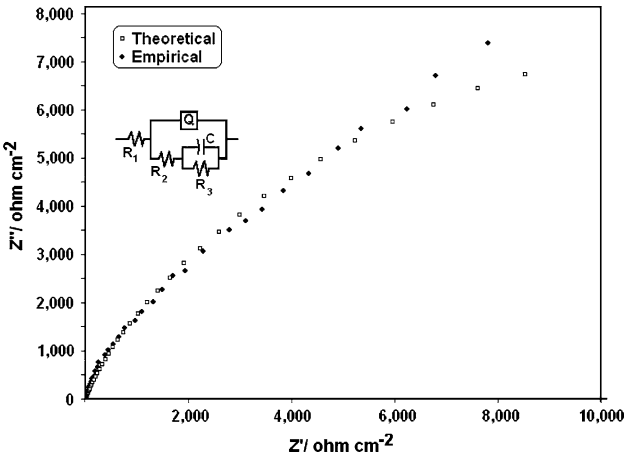

Fig. 11 Experimental and simulated Nyquist diagrams of Au in Ringer solution

The capacitive loop tends to close up in the Nyquist diagram of CrNi alloy (Fig. 10). This verifies the presence of a compact non-conductive surface film.

The EIS data of Au alloy (Fig. 11) are almost the same as those of the Cr Ni alloy indicating the formation of a compact non conducting oxide layer. The fact that Au gives the best result with Ti6Al4V alloy can be explained by the better covering nature of the oxide layer formed.

According to Tafel and EIS data the best couple for dental applications is Ti–Au. The corrosion parameters of Ti–CrNi and Ti–CoCr couples are very close to each other.

Acknowledgments The authors are grateful to Gazi University Research Fund (Project no:04/2003-14 and 04/2005-11) for financial support.

References

1. Rack HJ, Qazi JI (2006) Mater Sci Eng C 26:1269–1277
2. Chu C, Xue X, Zhu J et al (2006) Mater Sci Eng A 429:18–24
3. Toumelin-Chemla F, Rouelle F, Burdairon G (1996) J Dent 24:109–115
4. Williams DF (1981) In: Williams DF (ed) Biocompatibility of clinical implant materials, vol 2. CRC Press, Boca Raton
5. Luckey HA, Kubli A Jr (1983) Titanium alloys in surgical implants STP 796. American Society for Testing and Materials, New York
6. Hanson M, Anderko K (1958) Constitution of binary alloys. McGraw-Hill, New York
7. Reclarua L, Lerfb R, Eschlera PY et al (2002) Biomaterials 23:3479–3485
8. Schutz RW (1986) Titanium; process industries corrosion–the theory and practice. National Association of Corrosion Engineers, Houston
9. Hille GH (1966) J Mater 1:373–383
10. Katzer A, Hockertz S, Buchhorn GH et al (2003) Toxicology 190:145–154

11. Mirza Rosca JC, Gonzalez S, Llorente ML et al (1997) 7th European Conference on Applications of Surface and Interface Analysis. Wiley, New York
12. Popa MV, Vasilescu E, Mirza Rosca JC et al (1997) Adv Mater Processing Tech 2:737
13. Popa MV, Radovici O, Vasilescu E, et al (1997) 9th Proceedings of the international metallurgy and materials Congress, vol I
14. Souza MEP, Ballester M, Freire CMA (2007) Surf Coat Tech 201:7775–7780
15. Blackwood DJ, Peter LM, Williams DE (1988) Electrochim Acta 33:1143–1149
16. Reclaru L, Meyer JM (1994) J Dent 22:159–168
17. Reclaru L, Meyer JM (1998) Biomaterials 19:85–92
18. Tomashov ND, Chernova GP, Ruscol YS et al (1974) Electrochim Acta 19:159–172
19. Bianco PD, Ducheyne P, Cuckler JM (1996) J Biomed Mater Res 31:227–234
20. Jacobs JJ, Skipor AK, Patterson LM et al (1999) Clin Orthop 358:173–180
21. Hsu RWW, Yang CC, Huang CA, et al (2004) Mater Chem Phys 86:269–279
22. Gurappa I (2002) Mater Characterization 49:73–79
23. MacDonald D, McKubre M (1981) ASTM Spec Tech Pub 727:110–149
24. Frateur I, Cattarin S, Musiani M (2000) J Electroanal Chem 482:202
25. Blackwood DJ, Chua AWC, Seah KHW et al (2000) Corros Sci 42:481–503
26. Nakagawa M, Matsuya S, Udoh K (2002) J Dent Mater 21:83–92
27. Pan J, Thierry D, Leygraf C (1996) Electrochim Acta 41:1143–1153
28. Tomashov ND, Chernova GP, Ruscol YS et al (1974) Electrochim Acta 19:159–172
29. Badawy WA, Legamy SS, Ismail KH (1993) J Br Corr 28:136
30. Kolman DG, Scully JR (1994) J Electrochem Soc 141:2633
31. Pan J, Thierry D, Leygraf C (1994) J Biomed Mater Res 28:113–122
32. Mansfeld F (1993) Analysis and interpretation of EIS data for metals and alloys. Chapter 4, Technical Report 26, Solartron–Schlumberger
33. MacDonald D, McKubre M (1981) Electrochemical impedance techniques in corrosion science, electrochemical corrosion testing. ASTM Spec Tech. Pub, New York